Journal of
NANOSCIENCE and NANOTECHNOLOGY

Editor-in-Chief: Hari Singh Nalwa, USA
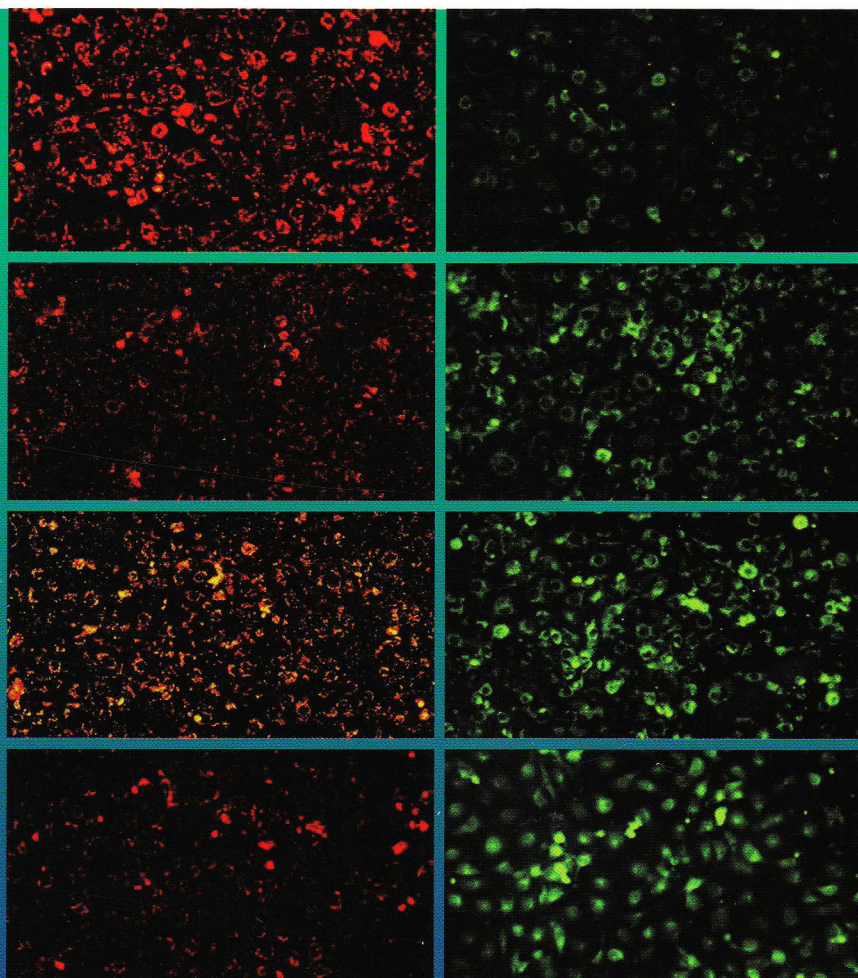
A Special Section on

International Conference on Nanotoxicology (ICNT2008)

GUEST EDITORS: Yuliang Zhao and Pingkun Zhou

A Facile Synthesis of Novel Self-Assembled Gold Nanorods Designed for Near-Infrared Imaging

Dipanjan Pan[1,*], Manojit Pramanik[2], Angana Senpan[1], Samuel A. Wickline[1,2], Lihong V. Wang[2,*], and Gregory M. Lanza[1,2]

[1] C-TRAIN and Division of Cardiology, Washington University School of Medicine, St. Louis, MO, 63108, USA
[2] Department of Biomedical Engineering, Washington University in St. Louis, Campus Box 1097, One Brookings Drive, St. Louis, MO 63130, USA

Molecular imaging techniques now allow recognition of early biochemical, physiological, and anatomical changes before manifestation of gross pathological changes. Photoacoustic imaging represents a novel non-ionizing detection technique that combines the advantages of optical and ultrasound imaging. Noninvasive photoacoustic tomography (PAT) imaging in combination with nanoparticle-based contrast agents show promise in improved detection and diagnosis of cardio-vascular and cancer related diseases. In this report, a novel strategy is introduced to achieve self-assembled colloidal gold nanorods, which are constrained to the vasculature. Gold nanorods (2–4 nm) were incorporated into the core of self-assembled lipid-encapsulated nanoparticles (sGNR) (~130 nm), providing more than hundreds of gold atoms per nanoparticle of 20% colloid suspension. The physico-chemical characterization in solution and anhydrous state with analytical techniques demonstrated that the particles were spherical and highly mono dispersed. In addition to the synthesis and characterization, sensitive near-infrared photoacoustic detection was impressively demonstrated in vitro.

Keywords: Photoacoustic Tomography, Nanobeacons, Gold Nanorod, Surface Plasmon Resonance, Near Infrared Imaging.

1. INTRODUCTION

Nanotechnology is permeating through the realms of science.[1–3] In the biomedical arena nanoparticles present a multiplicity of opportunity to diagnose pathology earlier or to deliver drug locally with greater safety margins. These image-guided therapeutic systems, so called theranostics, constitute a major pathway toward the concept of personalized medical management.[4,5] Novel nanoplatforms are being reported for all clinically relevant and emergent biomedical imaging modalities.[6–10] One particular promising new diagnostic imaging technology is photoacoustic (PA) tomography (PAT).

The capabilities of ultrasound have recently been expanded by the development of photoacoustic tomography also referred to as optoacoustic imaging.[7] PAT enhances traditional ultrasound images by introducing optical acoustic stimulation to ultrasonic imaging in order to reveal vascular patterns and oxygen saturation levels.[8,11–18] To date, PAT contrast agents have included single wall carbon nanotubes (SWNTs) targeting integrin $\alpha_v\beta_3$ and gold nanocages.[9,10,14,19–21] In contradistinction to the homing individual gold particles, we report a high payload gold nanorod (GNR) approach that provides marked signal amplification for robust PAT imaging.

Gold particles are excitable in near-infrared (NIR) range within the "optical transmission window" of the biological tissues ($\lambda = 650–900$ nm), which allows for deeper light penetration, lower autofluorescence, and reduced light scattering. Unlike small molecule fluorophores that can be excited in the NIR range using single- or two-photon excitation.[22–24] Gold particles are not susceptible to photobleaching, which has led to rapid growth for their bioapplications for sensing, heating, labeling and delivery. In the present approach to targeted PAT nanoagents, rod-shaped gold nanoparticles (i.e., nanorods) (GNR) offer distinct optical properties resulting from two surface plasmon (SP) bands corresponding to the transverse and longitudinal SP bands in the visible ($\lambda = 520$ nm) and the NIR regions, respectively, are of particular interest.[22–24] Owing to the presence of a relatively large extinction coefficient, gold nanorods present ideal opportunities for fluorescence,

light scattering, and two-photon luminescence imaging. We hypothesized that these properties would promote excellent contrast for photoacoustic bio-imaging in the NIR.

2. METHODS

2.1. Materials

Unless otherwise listed, all solvents and reagents were purchased from Aldrich Chemical Co. (St. Louis, MO) and used as received. Anhydrous chloroform was purchased from Aldrich Chemical Co. and distilled over calcium hydride prior to use. Biotinylated dipalmitoyl-phosphatidylethanolamine and high purity egg yolk phosphatidylcholine were purchased from Avanti Polar Lipids, Inc. Coated gold nanorods were purchased and used as received from Nanopartz, Inc. Argon and nitrogen (UHP, 99.99%) were used for storage of materials. The Spectra/Por membrane (Cellulose MWCO: 20000 Da) used for dialysis was obtained from Spectrum Medical Industries, Inc. (Laguna Hills, CA). Glutaraldehyde, osmium tetroxide, and uranyl acetate purchased from Electron Microscopy Sciences Tannic acid purchased from Sigma-Aldrich. Polybed 812 was purchased from Polysciences.

2.2. Typical Procedure for Preparation of *sGNR*

In a typical experimental procedure, gold nanorods (axial diameter: 25 ± 5 nm, length: 80 ± 8 nm) were suspended in almond oil (4 mL) and vigorously vortexed to homogeneity. The suspension was filtered through a small bed of cotton. The solvent was evaporated under reduced pressure at 60 °C. the surfactant co-mixture included high purity egg yolk phosphatidylcholine (90 mole%, 559 mg), cholesterol (8 mole%, 27 mg), and biotinylated-dipalmitoyl phosphatidylethanolamine (2 mole%, 15 mg). The surfactant co-mixture was dissolved in chloroform, filtered and evaporated under reduced pressure, dried in a 40 °C vacuum oven overnight, and dispersed into water by probe sonication. This suspension is combined with the gold nanorod-almond oil mixture (20% v/v), distilled deionized water (77.3% w/v), and glycerin (1.7%, w/v). The mixture was continuously processed thereafter at 20,000 PSI for 4 min with an S110 Microfluidics emulsifier (Microfluidics) at 4 °C. The nanobeacons were dialyzed against water using a 20,000 Da MWCO cellulose membrane for a prolonged period of time and then passed through a 0.45 μm Acrodisc Syringe filter. To prevent bacterial growth the nanobeacons are stored under argon atmosphere typically at 4 °C.
DLS (D_{av})/nm $= 129 \pm 07$ nm; AFM (H_{av})/nm $= 60 \pm 24$ nm; TEM (D_{ah})/nm $= 105 \pm 28$ nm; Zeta (ζ)/mV $= -41 \pm 12$ mV; PDI: 0.06 ± 0.02; ICP-MS $= 8.12$ μg of gold/g.

2.3. Photoacoustic Imaging System

A reflection-mode PA imaging system[25] was used for all PA experiments (Scheme 1). A tunable Ti:sapphire laser (LT-2211A, LOTIS TII) pumped by Q-switched Nd:YAG (LS-2137, LOTIS II) laser was the light source, providing <15 ns pulse duration and a 10 Hz pulse repetition rate. A dark-field ring-shaped illumination was used.[26] The light energy on the sample surface was controlled to conform to the American National Standards Institute (ANSI) standard for maximum permissible exposure (MPE).[27] A 5 MHz central frequency, spherically focused (2.54 cm focus length, 1.91 cm diameter active area element, and 72% bandwidth) ultrasonic transducer (V308, Panametrics-NDT) was used to acquire the generated PA signals. The signal was then amplified by a low-noise amplifier (5072PR, Panametrics-NDT), and recorded using a digital oscilloscope (TDS 5054, Tektronix) with a 50 mega-sampling rate. PA signal fluctuations due to pulse-to-pulse energy variation were compensated by signals from a photodiode (DET110, Thorlabs), which sampled the energy of each laser pulse.

A linear translation stage (XY-6060, Danaher Motion) was used for raster scanning to obtain three-dimensional (3-D) PA data. A computer controlled the stage and synchronized it with the data acquisition. To shorten the data acquisition time, a continuous scan was used without signal averaging. An A-line (A-scan) was the PA signal obtained along the depth direction at a single point. Multiple A-lines [acquired by a one-dimensional (1-D) scan] gave a two-dimensional (2-D) B-scan. A 3-D image was acquired with a 2-D scan. A 1-D depth-resolved image was obtained by multiplying the time axis of the initial A-scan (resolved in time along the depth direction) by the speed of sound in soft tissue (~1500 m/s).

The scanning time depends on the laser pulse repetition rate (PRR), the scanning step size, and the field of view (FOV). Typical values are a scanning step size for a 1-D scan $= 0.1$ mm, for a 2-D scan $= 0.2$ mm, a laser PRR $= 10$ Hz, and a FOV $= 15$ mm $\times$ 8 mm. The acquisition time $= \sim 14$ min for a 3-D image. Please note that no signal averaging was done for any of these images. The
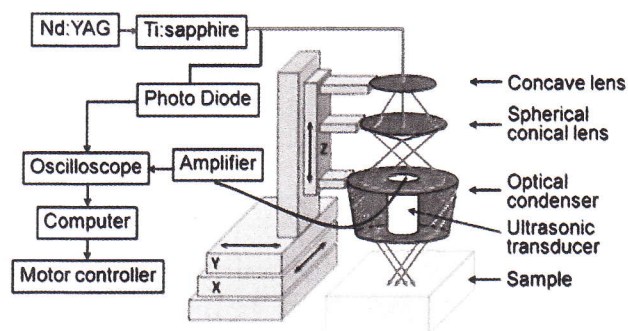
Scheme 1. Schematic diagram of the reflection-mode photoacoustic system.

transducer was located inside a water container with an opening of 5 cm × 5 cm at the bottom, sealed with a thin, clear membrane. The object was placed under the membrane, and ultrasonic gel was used for coupling the sound.

2.4. Dynamic Light Scattering Measurements

Hydrodynamic diameter distribution and distribution averages for the *sGNR* and controls in aqueous solutions were determined by dynamic light scattering. Hydrodynamic diameters were determined using a Brookhaven Instrument Co. (Holtsville, NY) Model Zeta Plus particle size analyzer. Measurements were made following dialysis (MWCO 10 kDa dialysis tubing, Spectrum Laboratories, Rancho Dominguez, CA) of *sGNR* suspensions into deionized water (0.2 μM). Nanorods were dialyzed into water prior to analysis. Scattered light was collected at a fixed angle of 90°. A photomultiplier aperture of 400 mm was used, and the incident laser power was adjusted to obtain a photon counting rate between 200 and 300 kcps. Only measurements for which the measured and calculated baselines of the intensity autocorrelation function agreed to within +0.1% were used to calculate nanoparticle hydrodynamic diameter values. All determinations were made in multiples of five consecutive measurements.

2.5. Electrophoretic Potential Measurements

Zeta potential (ζ) values for the *sGNR* were determined with a Brookhaven Instrument Co. (Holtsville, NY) model Zeta Plus zeta potential analyzer. Measurements were made following dialysis (MWCO 20 kDa dialysis tubing, Spectrum Laboratories, Rancho Dominguez, CA) of *sGNR* suspensions into water. Data were acquired in the phase analysis light scattering (PALS) mode following solution equilibration at 25 °C. Calculation of ζ from the measured nanoparticle electrophoretic mobility (μ) employed the Smoluchowski equation: $\mu = \varepsilon\zeta/\eta$, where ε and η are the dielectric constant and the absolute viscosity of the medium, respectively. Measurements of ζ were reproducible to within ±4 mV of the mean value given by 16 determinations of 10 data accumulations.

2.6. UV-Visible Spectroscopy

Absorption measurements were made with a Shimadzu UV-1601 P/N 206-67001 spectrophotometer using Shimadzu-UV probe 2.21 software.

2.7. Transmission Electron Microscopy Measurements

Nanoparticles fixed with 2.5% gluturaldehyde in PBS for 30 minutes on ice, were spun at top speed in a table top microfuge to form a tight pellet. After rinsing, the pellet was sequentially stained with osmium tetroxide, tannic acid, and uranyl acetate; then dehydrated and embedded in Polybed 812. Tissue was thin sectioned on a Reichert-Jung Ultracut, post stained in uranyl acetate and lead citrate, viewed on a Zeiss 902 Electron Microscope, and recorded with Kodak E.M. film.

2.8. Atomic Force Microscopy Measurements

A Digital Instruments Dimension 3000 series AFM (calibration date 08/2008) and standard Veeco tapping mode silicon probes w/PtIr coating were used for scanning the samples.

In a typical methodology, aqueous suspensions of *sGNR* samples were dried in a class 10000-clean room on a clean glass slide for 3 h. Once dried, samples were placed on the AFM and scanned. Pertinent scanning parameters were as follows: Resonant frequency (probe): 60–80 kHz; Example of tip velocity: (4 μm/s for 2μm), (15 μm/s for 5 μm), (30 μm/s for 10 μm). Aspect ratio: 1:1; Lift height: 20 nm; Resolution: 512 samples/line, 256 lines. The average particle height (H_{av}) values and standard deviations were generated from the analyses of a minimum of 100 particles from three micrographs.

2.9. Inductively Coupled Plasma-Optical Emission Spectroscopy

After imaging, the gold content of *sGNR* was analyzed by inductively coupled plasma-optical emission spectroscopy (ICP-MS, SOP7040, Rev 9) conducted at the Exova (formerly Bodycote), West Coast Analytical Service (WCAS), Santa Fe Springs, CA. Briefly, the samples were analyzed by a Leeman Labs Direct Reading Echelle ICP-MS, or a DRE instrument which was designed to handle sub-ppm to percent level metal concentrations.

3. RESULTS AND DISCUSSION

We report for the first time the development of a self-assembled, phospholipids-encapsulated gold nanorod system, carrying multiple numbers of tiny rods for efficient NIR imaging. The design of the self-assembled gold nanorods (*sGNR*) nanoparticles is based on the self-assembly of natural amphilies in aqueous media to entrap hundreds of gold atoms. A unique but simple strategy was followed that allowed us to entrap gold nanorods within the core matrix to avoid unfavorable interactions with surface homing ligands or surrounding plasma proteins. The self-assembled nanoparticles are encapsulated by phospholipids and are constrained to the vasculature by size (>120 nm) to increase the target specificity and avoid extravasation into non-target, non-clearance tissues. In a typical procedure, coated gold nanorods (GNR; transmission electron microscope axial diameter: 25 ± 5 nm, length: 80 ± 8 nm; λLSPR: 750 nm, λTSPR: 530 nm) were dispersed in chloroform and premixed with vegetable

oil (20% v/v almond oil) core matrix. The chloroform was removed under reduced pressure at 45 °C to form a suspension of gold nanorods in vegetable oil-based core matrix. In a parallel step, phospholipids were dissolved in chloroform, filtered and evaporated to dryness under reduced pressure to form a lipid-thin film mixture. The surfactant mixture comprised of phosphatidylcholine (PC) (99 mol%) and biotin-caproyl-PE (1%) (Scheme 2) for future bio-application. Lipid thin film mixture was dispersed in water (0.2 μM) and homogenized with the GNR suspension at 20000 psi for 4 min to produce self-assembled gold nanorods (Scheme 2). The particle thus formed was immediately subjected to dialysis against nanopure water using cellulosic membrane (20 KDa MW CO). This synthesis resulted in an encapsulation of ~127 gold atoms (ICP-MS = 8.12 μg of gold/g) and nominally 800 biotins per nanoparticle for biotin–avidin interaction.

The *sGNR* particles, thus formed, had nominal hydrodynamic diameter of 129 ± 7 nm as measured by dynamic light scattering (DLS). The polydispersity and zeta potential were measured as 0.06 ± 0.02 and -41 ± 12 mV (Brookhaven Instrument Co.), respectively. The large negative zeta potential implied successful phospholipids encapsulation and high colloidal stability of these nanoparticles. The dehydrated state diameter (Dav) and height parameters (Hav) of the *sGNR* were 105 ± 28 and 60 ± 24 nm, as measured by transmission electron microscopy (TEM) and atomic force microscopy measurements (AFM)

respectively (Fig. 1). The discrepancies in hydrodynamic diameter (DLS) and height values (AFM) was presumably due to the partial flattening of the nanoparticles on the glass substrates, which is indicative of the soft, compressible nature of these nanoparticles. TEM images of the *sGNR* confirmed the presence of multiple GNRs within the phospholipids encapsulated particles. AFM images pointed towards the spherical nature of the particles.

To assess the application of *sGNR* as NIR imaging probes *in vitro*, we attempted to detect the PA signals of *sGNR* from a tube (Silastic® laboratory tubing, Dow Corning Corp., with 300 μm inner diameter and 640 μm outside diameter) using a photoacoustic imaging system. Figure 2(a) shows the PA signals (excitation wavelength = 728 nm) obtained from a tube filled with *sGNR* (red) and a tube filled with water (blue). A very weak signal from the tube filled with water (blue) confirmed that there was no significant PA signal generated from either water or the tube surface and all the signals generated from the tube filled with *sGNR* were coming from the *sGNR* itself. At this excitation wavelength, the peak-to-peak PA signal amplitude obtained from *sGNR* was about 325 mV, compared to only 37 mV PA signal generated from the tube filled with water. The PA spectrum of the *sGNR* over the 728–810 nm window is shown in Figure 2(b). It can be seen that as the light wavelength increases, the absorptioncoefficient of *sGNR* decreases. Figure 2(c) shows a maximum amplitude
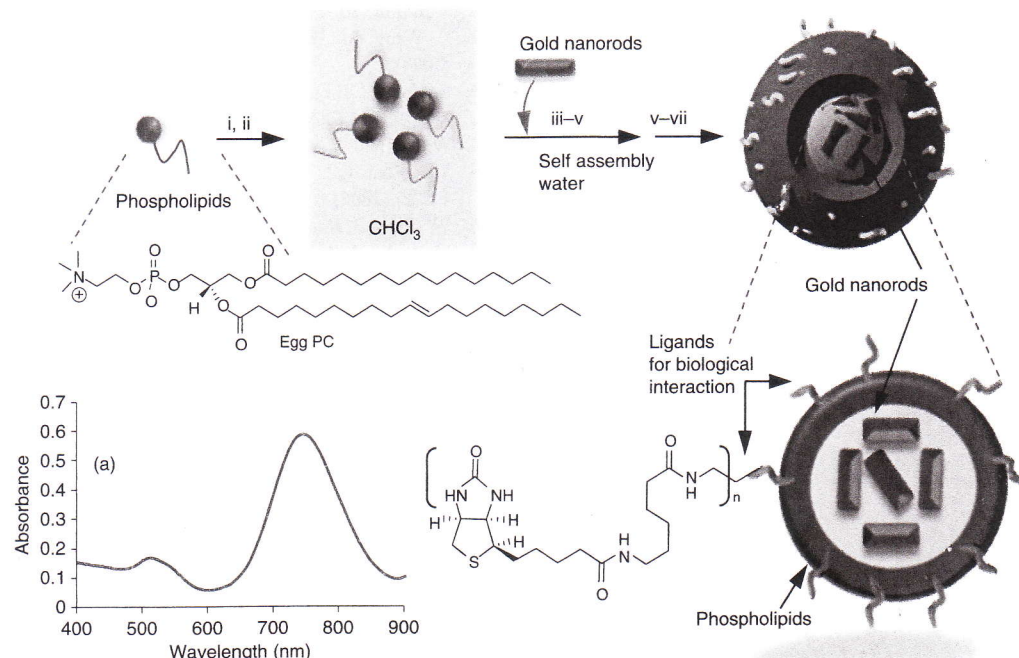
Scheme 2. Synthesis of self-assembled gold nano rods: (i) chloroform (ii) evaporation of chloroform under reduced pressure, 45 °C , thin film formation from phospholipids mixture; (iii) suspended with vegetable oil (2 w/v%), (iv) vortex, mixing; evaporation of chloroform under reduced pressure, 45 °C; (v) self-assembly (dispersion) in water by probe sonication at ambient temperature; (vi) homogenization, 20000 psi, 4 min, 0 °C; (vii) dialysis against nanopure water, 20 KDa MW CO cellulosic membrane. (a) UV-vis spectrum of gold nanorods showing LSPR and TSPR bands at 750 nm and 530 nm respectively.

AFM Images
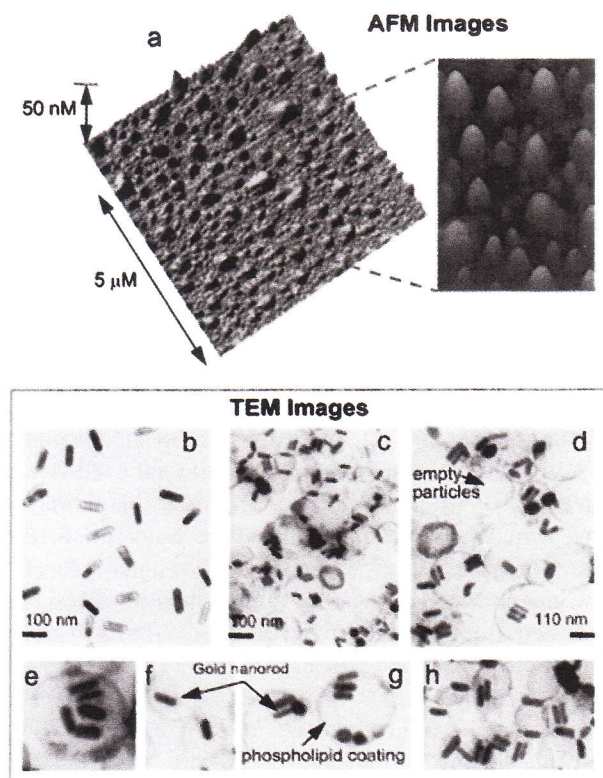
TEM Images

Fig. 1. Anhydrous state morphology of the *s*GNR nanoparticles: (a) AFM images of *s*GNR drop deposited over glass; (b) TEM image of GNR drop deposited over Ni-grid; (c–d) TEM images of *s*GNR drop deposited over Ni-grid; (e–h) specific sections of *s*GNR showing multiple localization of gold nanorods encapsulated by phospholipids.
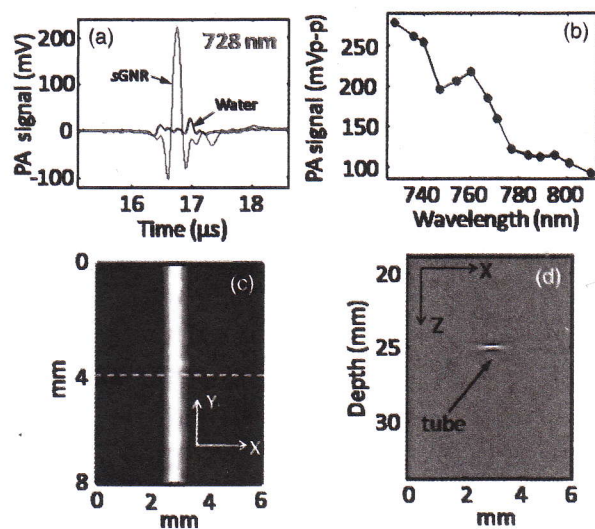
Fig. 2. Photoacoustic imaging of *s*GNR nanoparticles: (a) PA signals generated from a tube (Silastic® laboratory tubing, Dow Corning Corp., I.D. 300 μm, O.D. 640 μm) filled with *s*GNR; (b) PA spectrum of *s*GNR in the NIR window (728–810 nm); (c) Maximum amplitude projection (MAP)[18] photoacoustic image of a tube filled with *s*GNR; (b) PA B-scan image along the dotted line in (c), with the bright spot showing the PA signal originating from the tube filled with *s*GNR.

projection (MAP)[18] photoacoustic image of the same tube filled with *s*GNR (wavelength = 747 nm). Figure 2(d) shows the B-scan PA image along the dotted line in 2(c) and the strong PA signal from *s*GNR is marked with an arrow.

4. CONCLUSIONS

The strong PA signal from *s*GNR in the NIR region indicates the potential for molecular PA imaging of this platform. This work introduced the concept of a "soft" type self-assembled gold nanorod contrast agent for efficient NIR optical detection. Further *in vitro* and *in vivo* works are warranted to realize the full potential of the platform to improve photoacoustic detection of diseased sites.

References and Notes

1. D. Pan, G. M. Lanza, S. A. Wickline, and S. D. Caruthers, *Eur. J. Radiol.* 70, 274 (**2009**).
2. L. Wang, M. B. O'Donoghue, and W. Tan, *Nanomedicine* 1, 413 (**2006**).
3. S. Nie, Y. Xing, G. J. Kim, and J. W. Simons, *Annu. Rev. Biomed. Eng.* 9, 257 (**2007**).
4. W. Cai and X. Chen, *Small* 3, 1840 (**2007**).
5. V. P. Zharov, J. W. Kim, D. T. Curiel, and M. Everts, *Nanomedicine* 1, 326 (**2005**).
6. W. Chen, *J. Nanosci. Nanotechnol.* 8, 1019 (**2008**).
7. M. L. Li, J. T. Oh, X. Y. Xie, G. Ku, W. Wang, C. Li, G. Lungu, G. Stoica, and L. H. V. Wang, *Proc. IEEE* 96, 481 (**2008**).
8. X. D. Wang, Y. J. Pang, G. Ku, X. Y. Xie, G. Stoica, and L. H. V. Wang, *Nat. Biotechnol.* 21, 803 (**2003**).
9. A. Agarwal, S. W. Huang, M. O'Donnell, K. C. Day, M. Day, N. Kotov, and S. Ashkenazi, *J. Appl. Phys.* 102, 064701 (**2007**).
10. A. De La Zerda, C. Zavaleta, S. Keren, S. Vaithilingam, S. Bodapati, Z. Liu, J. Levi, B. R. Smith, T. J. Ma, O. Oralkan, Z. Cheng, X. Y. Chen, H. J. Dai, B. T. Khuri-Yakub, and S. S. Gambhir, *Nat. Nanotechnol.* 3, 557 (**2008**).
11. G. Peng, U. Tisch, O. Adams, M. Hakim, N. Shehada, Y. Y. Broza, S. Billan, R. Abdah-Bortnyak, A. Kuten, and H. Haick, *Nat. Nanotechnol.* 4, 669 (**2009**).
12. J. W. Kim, E. I. Galanzha, E. V. Shashkov, H. M. Moon, and V. P. Zharov, *Nat. Nanotechnol.* 4, 688 (**2009**).
13. K. H. Song, E. W. Stein, J. A. Margenthaler, and L. H. V. Wang, *J. Biomed. Opt.* 13, 054033 (**2008**).
14. K. H. Song, C. H. Kim, C. M. Cobley, Y. N. Xia, and L. H. V. Wang, *Nano Lett.* 9, 183 (2009).
15. R. A. Kruger, P. Y. Liu, Y. R. Fang, and C. R. Appledorn, *Med. Phys.* 22, 1605 (**1995**).
16. C. G. A. Hoelen, F. F. M. de Mul, R. Pongers, and A. Dekker, *Opt. Lett.* 23, 648 (**1998**).

17. A. A. Oraevsky, E. V. Savateeva, S. V. Solomatin, A. A. Karabutov, V. G. Andreev, Z. Gatalica, T. Khamapirad, and P. M. Henrichs, *Proc. SPIE* 4618, 81 (**2002**).
18. H. F. Zhang, K. Maslov, G. Stoica, and L. H. V. Wang, *Nat. Biotechnol.* 24, 848 (**2006**).
19. Y. W. Wang, X. Y. Xie, X. D. Wang, G. Ku, K. L. Gill, D. P. O'Neal, G. Stoica, and L. H. V. Wang, *Nano Lett.* 4, 1689 (**2004**).
20. M. Pramanik, M. Swierczewska, D. Green, B. Sitharaman, and L. H. V. Wang, *J. Biomed. Opt.* 14, 034018 (**2009**).
21. D. Pan, M. Pramanik, A. Senpan, X. Yang, K. H. Song, M. J. Scott, H. Zhang, P. J. Gaffney, S. A. Wickline, L. H. V. Wang, and G. M. Lanza, *Angew. Chem. Intl. Ed.* 48, 4170 (**2009**).
22. H. Kojima, *Yakugaku Zasshi.* 128, 1653 (**2008**).
23. V. Ntziachristos, C. Bremer, and R. Weissleder, *Eur. Radiol.* 13, 195 (**2003**).
24. B. C. Rostro-Kohanloo, L. R. Bickford, C. M. Payne, E. S. Day, L. J. Anderson, M. Zhong, S. Lee, K. M. Mayer, T. Zal, L. Adam, C. P. Dinney, R. A. Drezek, J. L. West, and J. H. Hafner, *Nanotechnology* 20, 434005 (**2009**).
25. K. H. Song and L. H. V. Wang, *J. Biomed. Opt.* 12, 060503 (**2007**).
26. K. Maslov, G. Stoica, and L. H. V. Wang, *Opt. Exp.* 30, 625 (**2005**).
27. Laser Institute of America, American National Standard for Safe Use of Lasers ANSI Z136.1-2000, American National Standards Institute, Inc., New York, NY (**2000**).

RESEARCH ARTICLE